Electronic supplementary information (ESI†)

Self-assembly optimization of cadmium/molybdenum sulfide hybrids by cation coordination competition toward extraordinarily efficient photocatalytic hydrogen evolution

Xiaoyong Xu,*[,a] Fengting Luo,[a] Gang Zhou,[c] Jingguo Hu,*[,a] Haibo Zeng,*[,b] and Yong Zhou*[,c]

[a]*School of Physics Science and Technology, Yangzhou University, Yangzhou 225002, China. E-mail: xxy@yzu.edu.cn, jghu@yzu.edu.cn*

[b]*Institute of Optoelectronics & Nanomaterials, Nanjing University of Science and Technology, Nanjing 210094, China. E-mail: zeng.haibo@njust.edu.cn*

[c]*School of Physics, Nanjing University, Nanjing 210093, China. E-mail: zhouyong1999@nju.edu.cn*

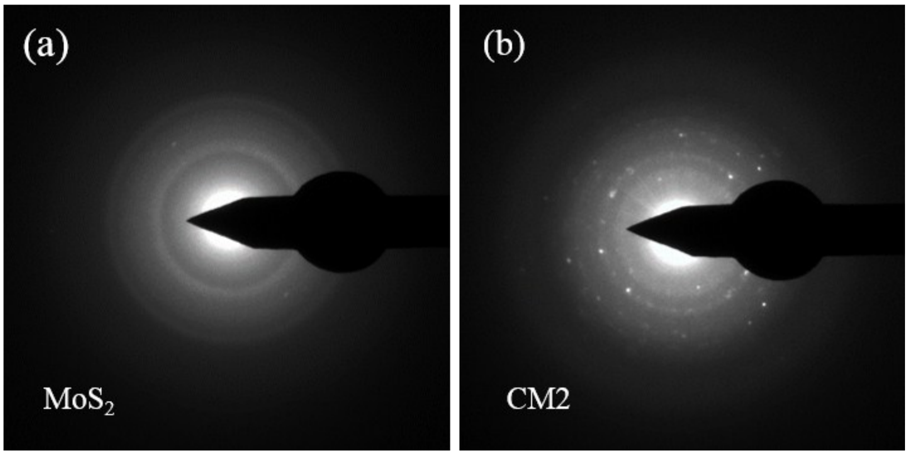

Fig. S1 SAED patterns of (a) MoS$_2$ and (b) CM2.

The comparison of the corresponding SAED patterns for pure MoS$_2$ and CM2 indicates the heterogeneous components in CM2 hybrid.

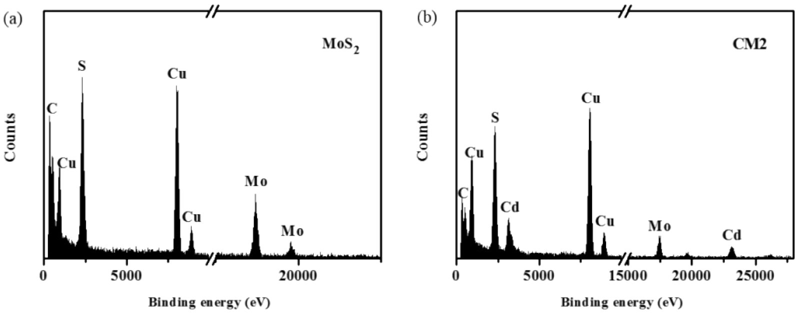

Fig. S2 EDX spectra of MoS$_2$ and CM2.

The comparison of the corresponding EDX spectra for pure MoS$_2$ and CM2 indicates the incorporation of Cd element in CM2 hybrid. And CM2 consists of Cd, S and Mo elements, while C and Cu elements come from the sample holder for TEM tests.

Table S1 Element proportion analysis for CM2 based on XPS data.

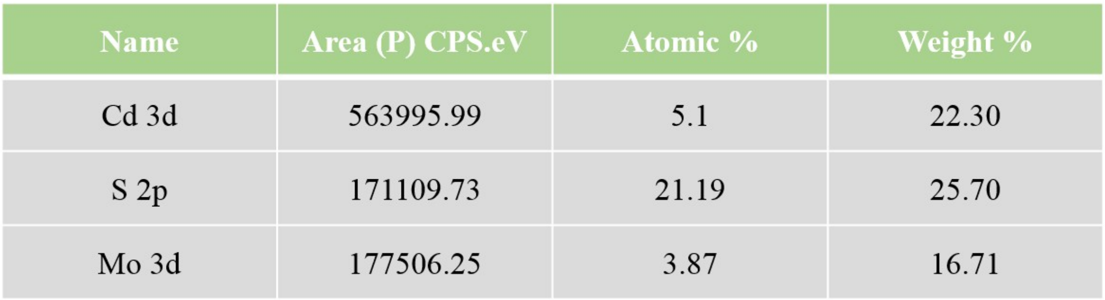

Name	Area (P) CPS.eV	Atomic %	Weight %
Cd 3d	563995.99	5.1	22.30
S 2p	171109.73	21.19	25.70
Mo 3d	177506.25	3.87	16.71

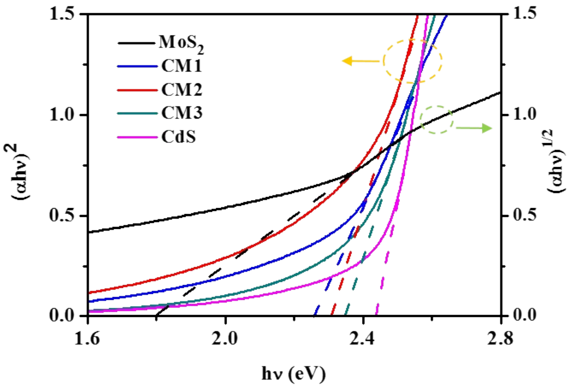

Fig. S3 Transformed reflectance spectra from UV-Vis absorption spectra of MoS_2, CdS and CM hybrids.

The corresponding Kubelka–Munk transformed reflectance spectra were used to determine the band-gap values for CM hybrids, as well as pure MoS_2 and CdS as two references. The monotonical tunability of the band gaps for CM hybrids is indicated to be associated with the energy-band coupling and the electronic interaction between CdS and MoS_2.

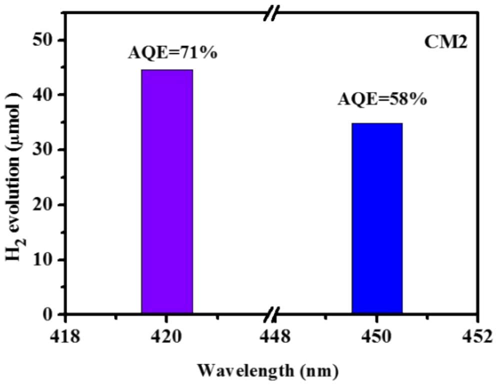

Fig. S4 Amount of evolved H_2 and corresponding AQE over CM2 photocatalyst under the monochromatic light irradiations of 420 and 450 nm for 10 h, respectively.

The AQE values were determined by the following calculation method:

$$\begin{aligned}\text{AQE [\%]} &= \frac{\text{number of reacted electrons}}{\text{number of incident photons}} \times 100\% \\ &= \frac{\text{number of evolved } \mathrm{H_2} \text{ molecules} \times 2}{\text{number of incident photons}} \times 100\% \\ &= \frac{M_{\mathrm{H_2}} \times N_{\mathrm{A}} \times 2 \times h \times c}{I_{\mathrm{i}} \times S \times t \times \lambda} \times 100\%\end{aligned}$$

where $M_{\mathrm{H_2}}$ is the mole number of evolved H_2, N_{A}, h are the Avogadro's and Planck's constants, c, λ, t, S and I_{i} are the wave speed, wavelength, time, area, and intensity of light irradiation, respectively. The I_{i} was determined by FZ-A spectroradiometer (Perfectlight, Beijing) and the S was calibrated to be 10 cm^2.

Table S2 Various parameters for AQE calculation.

Wavelength (nm)	Intensity (μW cm^{-2})	H_2 amount (μmol)
420 (±5 nm)	100	44.6
450 (±5 nm)	95	34.9

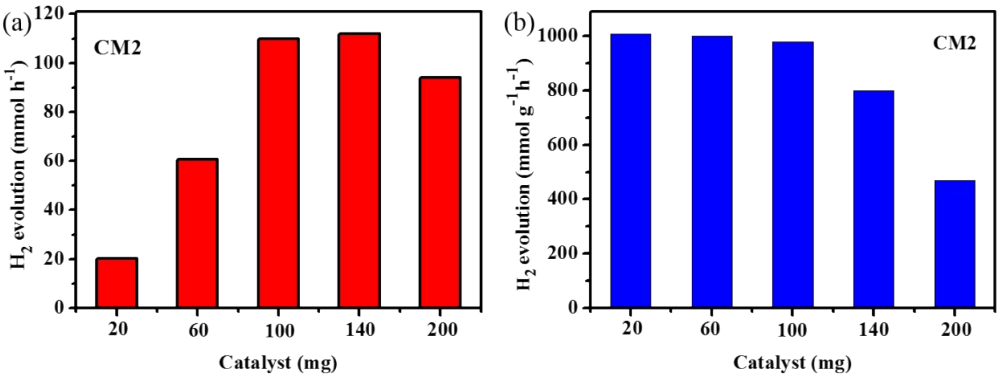

Fig. S5 H_2 evolution rates normalized to (a) time (per hour), and (b) mass and time (per gram per hour) at different catalyst concentrations.

With the catalyst dose increasing, the H_2 output per hour gradually increases, after that it instead decreases owing to the optical shielding effect induced by the excess suspended catalyst. Note that the H_2 evolution rates (mmol h^{-1} g^{-1}) normalized to the catalyst mass are very similar when the catalyst concentration is lower than 1 g L^{-1}, meaning that such a high photocatalytic activity is indeed intrinsic, while it suffers from shielding effect at related high catalyst concentration.

Table S3 Comparison of various MoS_2-CdS hybrids reported for photocatalytic H_2 evolution.

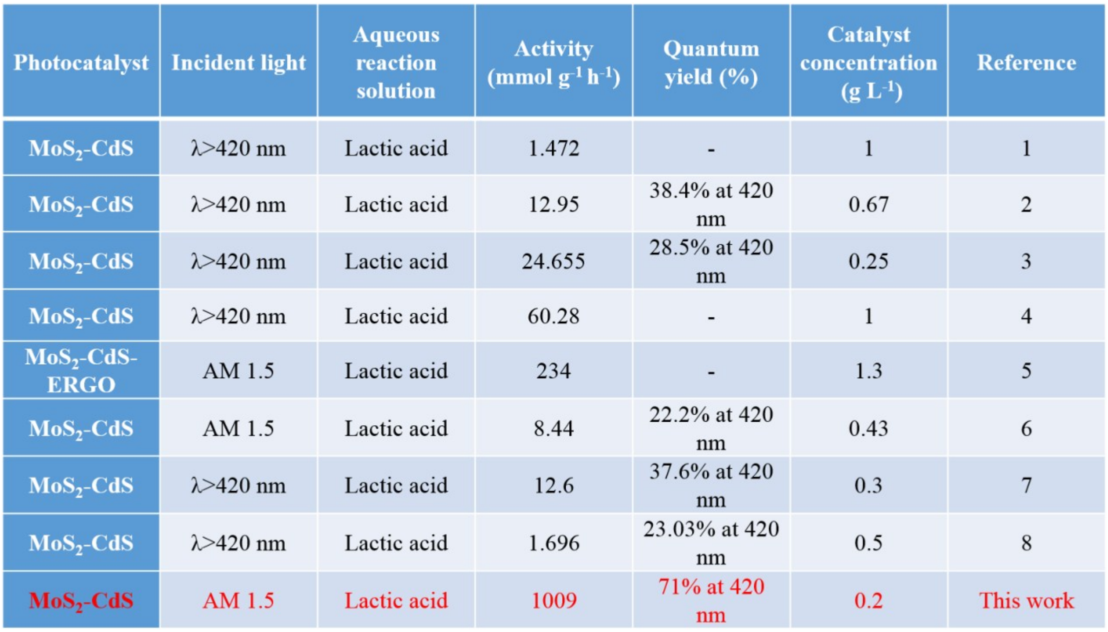

Photocatalyst	Incident light	Aqueous reaction solution	Activity (mmol g^{-1} h^{-1})	Quantum yield (%)	Catalyst concentration (g L^{-1})	Reference
MoS_2-CdS	λ>420 nm	Lactic acid	1.472	-	1	1
MoS_2-CdS	λ>420 nm	Lactic acid	12.95	38.4% at 420 nm	0.67	2
MoS_2-CdS	λ>420 nm	Lactic acid	24.655	28.5% at 420 nm	0.25	3
MoS_2-CdS	λ>420 nm	Lactic acid	60.28	-	1	4
MoS_2-CdS-ERGO	AM 1.5	Lactic acid	234	-	1.3	5
MoS_2-CdS	AM 1.5	Lactic acid	8.44	22.2% at 420 nm	0.43	6
MoS_2-CdS	λ>420 nm	Lactic acid	12.6	37.6% at 420 nm	0.3	7
MoS_2-CdS	λ>420 nm	Lactic acid	1.696	23.03% at 420 nm	0.5	8
MoS_2-CdS	AM 1.5	Lactic acid	1009	71% at 420 nm	0.2	This work

Table S4 Comparison of various state-of-the-art heterogeneous catalysts reported for photocatalytic H_2 evolution.

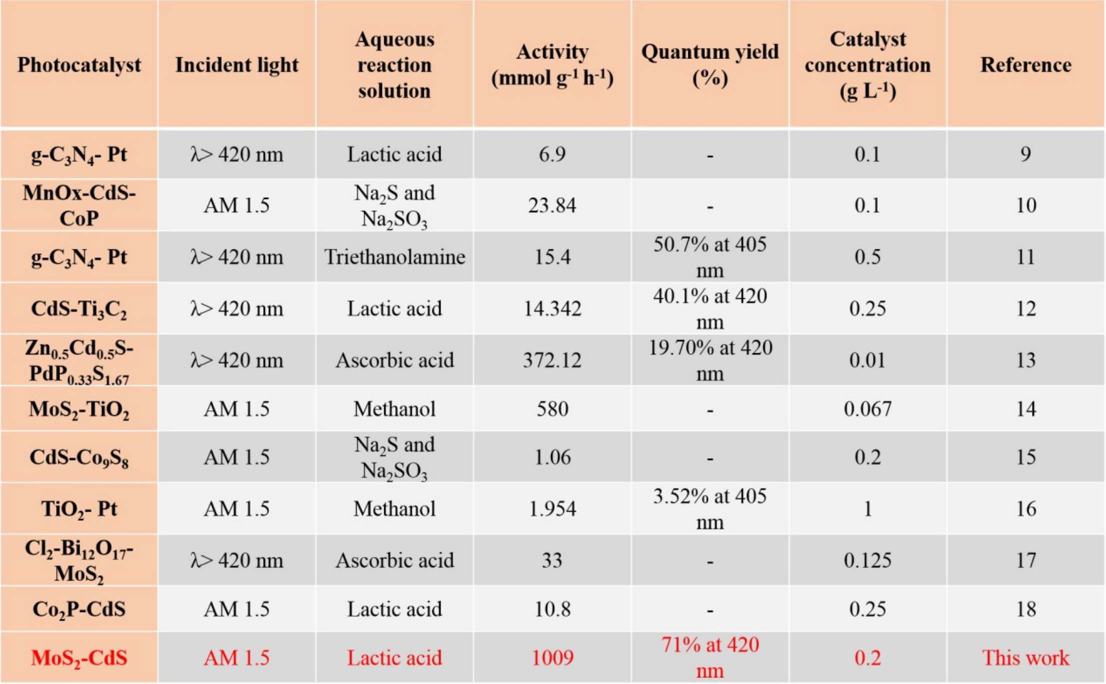

Photocatalyst	Incident light	Aqueous reaction solution	Activity (mmol g^{-1} h^{-1})	Quantum yield (%)	Catalyst concentration (g L^{-1})	Reference
g-C_3N_4- Pt	λ> 420 nm	Lactic acid	6.9	-	0.1	9
MnOx-CdS-CoP	AM 1.5	Na_2S and Na_2SO_3	23.84	-	0.1	10
g-C_3N_4- Pt	λ> 420 nm	Triethanolamine	15.4	50.7% at 405 nm	0.5	11
CdS-Ti_3C_2	λ> 420 nm	Lactic acid	14.342	40.1% at 420 nm	0.25	12
$Zn_{0.5}Cd_{0.5}S$-$PdP_{0.33}S_{1.67}$	λ> 420 nm	Ascorbic acid	372.12	19.70% at 420 nm	0.01	13
MoS_2-TiO_2	AM 1.5	Methanol	580	-	0.067	14
CdS-Co_9S_8	AM 1.5	Na_2S and Na_2SO_3	1.06	-	0.2	15
TiO_2- Pt	AM 1.5	Methanol	1.954	3.52% at 405 nm	1	16
Cl_2-$Bi_{12}O_{17}$-MoS_2	λ> 420 nm	Ascorbic acid	33	-	0.125	17
Co_2P-CdS	AM 1.5	Lactic acid	10.8	-	0.25	18
MoS_2-CdS	AM 1.5	Lactic acid	1009	71% at 420 nm	0.2	This work

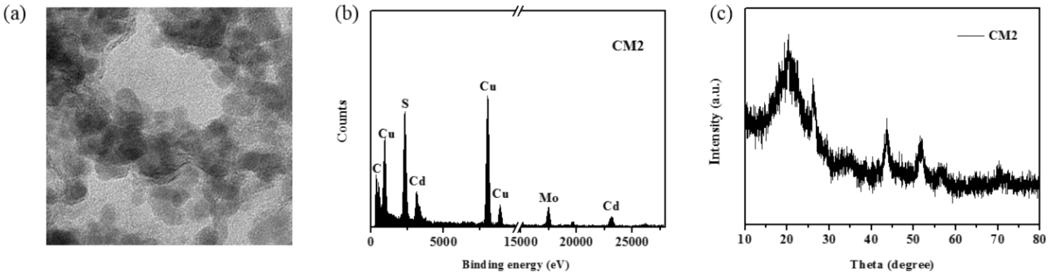

Fig. S6 (a) TEM image, (b) EDX spectrum and (c) XRD pattern of CM2 after stability testing.

The TEM image, XRD pattern and EDX spectrum of CM2 after stability testing were measured and together show no noticeable change in its microstructure, confirming the excellent stability of CM2 catalyst during photocatalytic reaction.

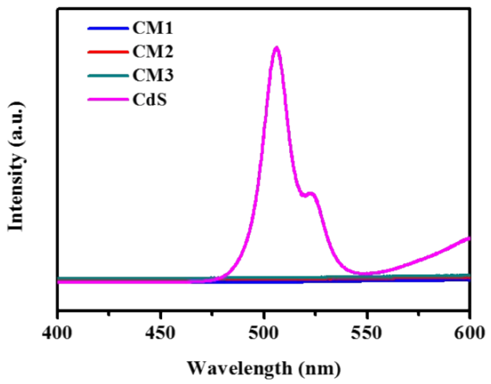

Fig. S7 Steady-state PL spectra of CM hybrids and pure CdS.

The steady-state PL spectra show the vanishing fulorescence in CM hybrids, compared to that of pure CdS, meaning the effective suppression against photogenerated charge recombination after CdS hybridized with MoS_2, which boosts exciton dissociation and hot electron output.

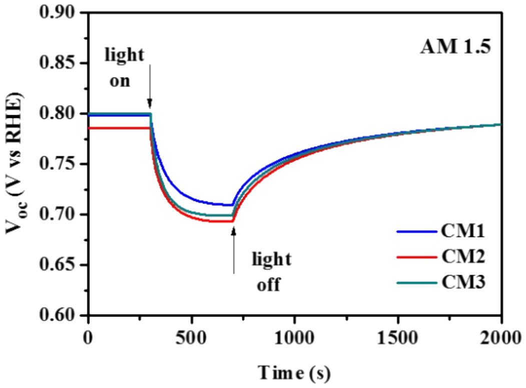

Fig. S8 Time dependent V_{oc} upon switching light irradiation of CM hybrids.

When the light irradiation at open circuit is terminated, electron recombination kinetics at the semiconductor interface is correlated to the photovoltage decay rate. The electron lifetimes (τ) at different potentials can be determined from the V_{oc} decay using the following equation:[19]

$$\tau = -\frac{k_B T}{e}\left(\frac{dV_{oc}}{dt}\right)^{-1}$$

where k_B is Boltzmann's constant, T is the temperature, and e is the elementary charge. The comparison of V_{oc} decay upon irradiation termination for CM hybrids revealed that the longer survivability of electrons in CM2, which results from the more effective electron transfer and separation at heterointerface in CM2.

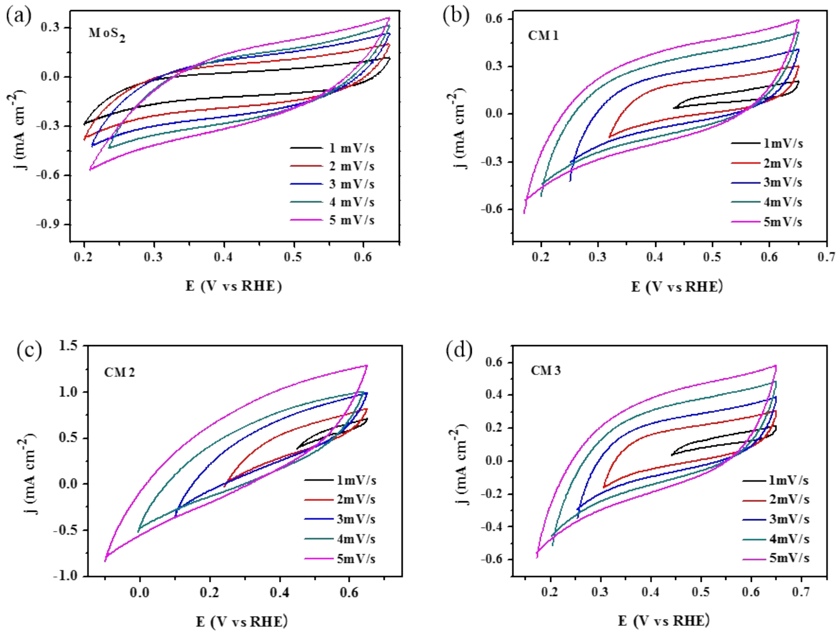

Fig. S9 Electrochemical CV curves at various scan rates for MoS_2 and CM hybrids.

The electrochemical CV was performed for different catalysts to estimate their effective surface areas. The potential ranges without faradic current was selected, which meant that the current response in this region was attributed to the charging of the double layer. The halves of the positive and negative current density differences at the center of the scanning potential ranges are plotted versus the voltage scan rates in Fig. 4d, in which the slopes are the eletrochecmical DLCs.

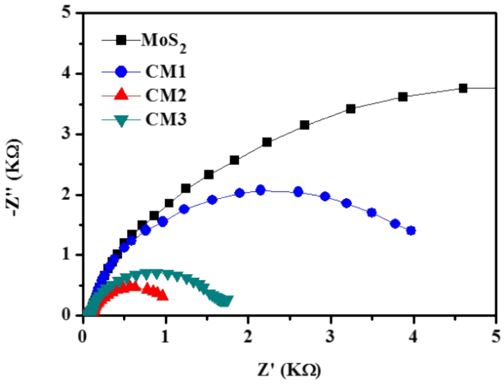

Fig. S10 EIS Nyquist plots for MoS_2 and CM hybrids.

The Nyquist plots reveal the smallest semicircle and the lowest interfacial electron transfer resistance in CM2, compared to those in CM1 and CM2. The more active sites equiped on CM2 effectively reduce the activation barrier, facilitating the interfacial electron transfer into HER.

References

1 J. Chen, X. J. Wu, L. S. Yin, B. Li, X. Hong, Z. X. Fan, B. Chen, C. Xue and H. Zhang, *Angew. Chem., Int. Ed.*, 2015, **54**, 1210.

2 K. Chang, M. Li, T. Wang, S. X. Ouyang, P. Li, L. Q. Liu and J. H. Ye, *Adv. Energy Mater.*, 2015, **5**, 1402279.

3 B, Han, S. Q. Liu, N. Zhang, Y. J. Xu and Z. R. Tang, *Appl. Catal. B: Environ.*, 2017, **202**, 298.

4 X. L. Yin, G. Y. He, B. Sun, W. J. Jiang, D. J. Xue, A. D. Xia, L. J. Wan and J. S. Hu, *Nano Energy*, 2016, **28**, 319.

5 D. P. Kumar, S. Hong, D. A. Reddy and T. K. Kim, *Appl. Catal. B: Environ.*, 2017, **212**, 7.

6 K. Zhang, J. K. Kim, M. Ma, S. Y. Yim, C. L. Lee, H.J. Shin and J. H. Park, *Adv. Funct. Mater.*, 2016, **26**, 4527.

7 K. Zhang, S. F. Qian, W. J. Kim, J. K. Kim, X. W. Sheng, J. Y. Lee and J. H. Park, *Nano Energy*, 2017, **34**, 481.

8 F. K. Ma, Y. Z. Wu, Y. L. Shao, Y. Y. Zhong, J. X. Lv and X. P. Hao, *Nano Energy*, 2016, **27**, 466.

9 H. J. Yu, R. Shi, Y. X. Zhao, T. Bian, Y. F. Zhao, C. Zhou, G. I. N. Waterhouse, L. Z. Wu, C. H. Tung and T. R. Zhang, *Adv. Mater.*, 2017, **29**, 1605148.

10 M. Y. Xing, B. C. Qiu, M. M. Du, Q. H. Zhu, L. Z. Wang and J. L. Zhang, *Adv. Funct. Mater.*, 2017, **27**, 1702624.

11 L. H. Lin, H. H. Ou, Y. F. Zhang and X. C. Wang, *ACS Catal.*, 2016, **6**, 3921.

12 J. R. Ran, G. P. Gao, F. T. Li, T. Y. Ma, A. J. Du and S. Z. Qiao, *Nat. Commun.*, 2017, **8**, 13907.

13 J. G. Song, H. T. Zhao, R. R. Sun, X. Y. Li and D. J. Sun, *Energy Environ. Sci.*, 2017, **10**, 225.

14 L. Guo, Z. Yang, K. Marcus, Z. Li, B. Luo, L. Zhou, X. Wang, Y. Du and Y. Yang, *Energy Environ. Sci.*, 2018, **11**, 106.

15 B. C. Qiu, Q. H. Zhu, M. M. Du, L. G. Fan, M. Y. Xing and J. L. Zhang, *Angew. Chem.*, 2017, **129**, 2728.

16 L. D. Li, J. Q. Yan, T. Wang, Z. J. Zhao, J. Zhang, J. L. Gong and N. J. Guan, *Nat. Commun.*, 2015, **6**, 5881.

17 J. Li, G. M. Zhan, Y. Yu and L. Z. Zhang, *Nat. Commun.*, 2016, **7**, 11480.

18 W. T. Bi, L. Zhang, Z. T. Sun, X. G. Li, T. Jin, X. J. Wu, Q. Zhang, Y. Luo, C. Z. Wu and Y. Xie, *ACS Catal.*, 2016, **6**, 4253.

19 J. S. DuChene, B. C. Sweeny, A. C. Johnston-Peck, D. Su, E. A. Stach and W. D. Wei, *Angew. Chem. Int. Ed.*, 2014, **53**, 7887.